Available online at www.sciencedirect.com
SCIENCE DIRECT®
Computer Coupling of Phase Diagrams and Thermochemistry 29 (2005) 7–16
www.elsevier.com/locate/calphad

A modified embedded atom method interatomic potential for carbon

Byeong-Joo Lee*, Jin Wook Lee

Department of Materials Science and Engineering, Pohang University of Science and Technology, Pohang 790-784, Republic of Korea

Received 11 November 2004; received in revised form 12 February 2005; accepted 13 February 2005
Available online 2 March 2005

Abstract

A semi-empirical interatomic potential for carbon has been developed, based on the modified embedded atom method formalism. The potential describes the structural properties of various polytypes of carbon, elastic, defect and surface properties of diamonds as satisfactorily as the well-known Tersoff potential. Combined with the Lennard-Jones potential, it can also reproduce the physical properties of graphite and amorphous carbon reasonably well. The applicability of the present potential to atomistic approaches on carbon nanotubes and fullerenes is also shown. The potential has the same formalism as previously developed MEAM potentials for bcc, fcc and hcp elements, and can be easily extended to describe various metal–carbon alloy systems.

Keywords: Semi-empirical interatomic potential; Modified embedded atom method; Carbon; Diamond; Graphite

1. Introduction

Not only as a pure element but also as an alloying element in metals, carbon is one of the most widely used elements. Atomic structure is an important factor for materials properties of carbon nanotubes, deposited diamond, amorphous carbon, etc. The distribution of carbon atoms in metallic interstitial solid solutions also has a decisive effect on the mechanical properties of the material. In order to be able to control material syntheses and properties, it is essential to understand atomic structural behavior and the governing rules involved in the atomic structural evolution of carbon atoms in various forms. One of the most effective ways to investigate the atomic structural behaviors of carbon atoms is to use atomistic simulation techniques based on semi-empirical interatomic potentials.

The essence of semi-empirical atomistic approaches is the reliability of the interatomic potential used. A reliable interatomic potential would reproduce various fundamental physical properties of relevant elements or alloys, such as elastic properties, structural properties, defect properties, surface properties, thermal properties. Another important characteristic of the semi-empirical atomistic approach is that it should be easy to extend the interatomic potential formalism to describe multi-component systems composed of various elements of different types (equilibrium structures). In order to be able to describe multi-component systems easily, it is essential to be able to describe individual elements using a common mathematical formalism.

To investigate the atomistic structural behaviors of carbon atoms, many (semi-)empirical interatomic potentials for carbon were developed, by Tersoff [1], Brenner [2], Heggie [3] and Andribet et al. [4]. The Tersoff potential was in good agreement with experimental data or first-principles calculations for the structural properties (cohesive energies and bond lengths of dimer and various solid structures), elastic properties (elastic constants of diamond) and point defect properties (vacancy formation and migration energies, and interstitial formation energies in diamond and graphite). However, for graphite, this potential considered only the in-plane interactions and could not describe interlayer interactions. Further, the potential formalism has been applied only to diamond structured elements, silicon [5], germanium [6] and carbon, and has never been applied to a metallic system.

* Corresponding author. Tel.: +82 54 279 2157; fax: +82 54 279 2399.
E-mail address: calphad@postech.ac.kr (B.-J. Lee).

0364-5916/$ - see front matter © 2005 Elsevier Ltd. All rights reserved.
doi:10.1016/j.calphad.2005.02.003

The Brenner potential was developed by modifying the Tersoff formalism so that it can better describe hydrocarbons. Recently, this potential has been upgraded by the original author and co-workers [7] so that it can better describe elastic properties, defect properties and surface properties for diamond to a similar degree to the Tersoff potential. The last two potentials were developed in an effort to overcome the limitations of the Tersoff potential in describing graphite structure. These potentials described the physical properties of graphite better than the Tersoff potential, but were not applied further to a wider range of elements.

In order to be able to investigate the effect of interstitial carbon on the structural and mechanical behaviors of metallic alloys or to investigate the atomic structure on metal/graphite or metal/carbon nanotube interfaces, it is necessary to develop an interatomic potential of carbon using a formalism that can also describe metallic elements and alloys. None of the above interatomic potential formalisms for carbon have been applied to a metallic system. The purpose of the present study is to provide a semi-empirical interatomic potential for carbon that describes the physical properties of pure carbon as satisfactorily as the Tersoff potential does, but using a formalism that can also describe metallic systems equally well. For the present purpose, the most recent version of the modified embedded atom method (MEAM) potential formalism [8,9] was selected. The MEAM showed the possibility that a single formalism can be applied to a wide range of elements including fcc, bcc, hcp, diamond-structured materials and even gaseous elements, in good agreement with experiments or first-principles calculations [10]. The MEAM was created by Baskes [10] by modifying the EAM [11,12] so that the directionality of bonding was considered. In the initial MEAM, the interactions among only first-nearest-neighbor atoms were considered. Recently, the MEAM was modified once again by one of the present authors and Baskes [8,9], so that the interactions among the second-nearest-neighbor atoms were partially considered and some critical shortcomings in the original MEAM were removed.

In the present paper, a brief description of the potential formalism, procedure for optimization of interatomic potential parameters and results of optimization will be reported. The applicability of the present potential to atomistic study on carbon nanotubes will also be demonstrated by comparing the computed relative stability, elastic property and defect property of some nanotubes with experiments or high level calculations.

2. Formalism and optimization of potential parameters

In the MEAM, the total energy of a system is approximated as

$$E = \sum_i \left[F_i(\overline{\rho}_i) + \frac{1}{2} \sum_{j(\neq i)} S_{ij}\phi_{ij}(R_{ij}) \right] \quad (1)$$

where F_i is the embedding function, $\overline{\rho}_i$ is the background electron density at site i, and S_{ij} and $\phi_{ij}(R_{ij})$ are the screening factor (see Appendix) and the pair interaction between atoms i and j separated by a distance R_{ij}, respectively. For general calculations of energy, the functional forms for the two terms on the right hand side of Eq. (1), F_i and ϕ_{ij}, should be given. The background electron density at a site is computed considering directionality in bonding. A specific form is given to the embedding function F_i, but not to the pair interaction ϕ_{ij}. Instead a reference structure where individual atoms are on the exact lattice points is defined, and the total energy per atom of the reference structure is estimated from the zero-temperature universal equation of state given by Rose et al. [13]. Then, the value of the pair interaction is evaluated from known values of the total energy per atom and the embedding energy, as a function of nearest-neighbor distance. In the original MEAM [10], only first-nearest-neighbor interactions are considered. The neglect of the second-nearest-neighbor and more distant neighbor interactions is effected by the use of a strong many-body screening function [14]. Consideration of the second-nearest-neighbor interactions in the modified formalism (the second-nearest-neighbor MEAM [8,9]) is effected by adjusting screening parameters, $C_{\min}$ and $C_{\max}$, so that the many-body screening becomes less severe. For computational convenience, in addition to the many-body screening function, a radial cutoff function is also applied [14]. Details of the MEAM formalism have been published in the literature [8–10,14], and are briefly introduced in the Appendix.

The 2NN (second-nearest-neighbor) MEAM formalism [9] gives fourteen independent model parameters for pure elements: four (E_c, R_e, B, d) for the universal equation of state, seven ($\beta^{(0)}$, $\beta^{(1)}$, $\beta^{(2)}$, $\beta^{(3)}$, $t^{(1)}$, $t^{(2)}$, $t^{(3)}$) for the electron density, one (A) for the embedding function and two ($C_{\min}$, $C_{\max}$) for many-body screening. Out of the fourteen parameters, E_c, R_e, and B are cohesive energy, nearest-neighbor distance, and bulk modulus of the reference structure, respectively. When a real structure is selected as the reference structure, these parameters become material properties, not model parameters, and the values can be obtained experimentally. In the present study, diamond structure was selected as the reference structure of MEAM carbon, and the values of the above three parameters were obtained from experimental information on diamond. For d, it was decided to give either 0 or 0.05, according to $(\partial B/\partial P)$ of individual reference structures [9]. However, for diamond, the $(\partial B/\partial P)$ value was not available. Based on that a very good agreement with the experimental value of $(\partial B/\partial P)$ could be obtained by setting $d = 0$ for MEAM silicon [15] which also has a diamond structure, a zero value was given to the d parameter of MEAM carbon in the present study. As has been done in the previous parameter optimizations for bcc [9] and fcc [16] metals using the 2NN MEAM, the $C_{\max}$ parameter was given a fixed value of 2.8. Therefore, the model

parameters of which values should be determined actually totalled nine, A, $\beta^{(0)}$, $\beta^{(1)}$, $\beta^{(2)}$, $\beta^{(3)}$, $t^{(1)}$, $t^{(2)}$, $t^{(3)}$ and $C_{\min}$. These parameter values were determined by fitting elastic constants and the vacancy formation energy of diamond, the elastic constant C_{11}, nearest-neighbor distance, stability and formation energy of graphite, and the nearest-neighbor distance and formation energy of dimer, simple cubic, bcc and fcc structures.

It was easy to fit a single property value exactly. However, it was not always possible to fit all target property values simultaneously. Because individual parameters did not have effects on all the target property values, by investigating which parameter has an effect on which property, an optimized set of parameters could be derived systematically.

Because the diamond structure was selected as the reference structure and the real E_c, R_e, and B values were used for the reference structure, with the present MEAM formalism the cohesive energy, the lattice constant and the bulk modulus of diamond could always be reproduced. However, it has been found often in empirical atomistic approaches that structures supposed to be stable up to melting collapse or transform to other unanticipated structures during molecular dynamics (MD) runs at finite temperatures. These stability problems happen because the parameter optimizations are mostly performed at 0 K, and the authors do not check the stability of the structures at finite temperatures. Also in the present work, all structural property calculations (cohesive energy and lattice parameter) were performed at 0 K. The bcc or fcc carbon, for example, may not be necessarily (meta)stable, and may collapse or transform to other structures at finite temperatures. However, this should not happen to the diamond structure. A simple stability test involves performing an MD run at a finite temperature and seeing whether the structure is kept or not. Such a test was done on a diamond structured sample composed of 512 atoms with periodic boundary conditions. The diamond structure was kept after 300,000 MD steps (300 ps) at 3000 K. It has been found in previous studies [8,9] that if a structure was not (meta)stable the collapse of the atomic structure occurred very soon, within several thousand MD steps. From all of these findings, it could be confirmed that the present MEAM diamond was indeed (meta)stable and did not cause the stability problem.

During parameter optimization a special effort was made to stabilize the graphite structure with correct formation energy and lattice constants. However, with only the present MEAM formalism it was difficult to obtain a graphite structure with correct lattice parameter values. In addition, considering that the bonding characters within each layer and between layers are different from each other, it was thought to be meaningless to try to describe in-plane and interlayer interactions in graphite using a common formalism. It seemed necessary to separate the in-plane and the interlayer interactions in graphite and describe these using different formalisms. The interlayer interaction in graphite is of van der Waals type. For this, the Lennard-Jones potential is suitable. Therefore, it was finally decided to describe the in-plane interaction using the MEAM formalism and the interlayer interaction using Lennard-Jones formalism. According to the 12–6 Lennard-Jones potential, the pair interaction between atoms i and j separated by a distance R_{ij} is given as follows:

$$\phi_{ij}^{L\text{-}J} = 4\varepsilon\left(\left(\frac{\sigma}{R_{ij}}\right)^{12} - \left(\frac{\sigma}{R_{ij}}\right)^{6}\right).$$

Here, ε and σ are parameters related to bond strength and bond length, respectively.

When both MEAM and Lennard-Jones potentials are used to describe the carbon potential, it is important to adjust the formalism so that the Lennard-Jones potential applies only to the interlayer interaction in graphite structure. For this, one more radial cutoff distance was defined. The interactions between atoms within this additional cutoff distance were described by the MEAM, and those between more distant atoms were described using the Lennard-Jones potential with an ordinary radial cutoff distance (arbitrarily 5.75 Å in the present study). The additional cutoff distance was selected to be 2.75 Å, which is larger than the second-nearest-neighbor distance (for 2NN MEAM, the radial cutoff distance should be larger than the second-nearest-neighbor distance) and smaller than the interlayer distance in graphite. By this means, the interlayer interactions in graphite could be accounted for only through the Lennard-Jones contribution. The Lennard-Jones contribution from in-plane atoms outside the additional cutoff distance could be removed by applying the same many-body screening as in the MEAM also to the Lennard-Jones potential. It should be mentioned here that one of the main differences between the MEAM and other empirical potentials is the use of many-body screening in the MEAM. At interatomic separations close to the radial cutoff distance, the interactions become negligible not because of the radial cutoff but because of the many-body screening. The additional cutoff distance 2.75 Å is a distance where in the graphite structure the Lennard-Jones interaction contributions as well as the MEAM contributions are completely removed due to the many-body screening.

For other structures (bcc, fcc, etc.), the additional cutoff distance 2.75 Å is large enough, and the interactions between atoms more distant than the additional cutoff distance are removed by the many-body screening. This means that it is not necessary to use the additional Lennard-Jones potential for these structures. Exactly the same results are obtained by using only the MEAM potential. In the present study, the combined MEAM + L-J potential was used only for the property calculation for graphite and for simulations on structural evolution where the graphite structure can appear (preparation of amorphous carbon). For the same reason (use of many-body screening), the MEAM formalism may be used alone, without combination with the L-J

potential, in future simulations for metal–carbon systems if the simulation does not involve the precipitation of graphite.

The additional Lennard-Jones parameters, ε and σ, were determined by fitting the elastic constant C_{33} and the equilibrium interlayer distance of graphite, respectively. The final set of parameters is listed in Table 1.

3. Calculation of physical properties

The carbon potential determined by the above procedure was used to compute various physical properties of carbon in order to evaluate its reliability. In addition to the properties that have been used for parameter optimization, many other structural, defect, surface and thermal properties were calculated, and are presented in this section. Through comparisons between the present calculations and experimental information or higher level calculations, the applicability and limits of the present potential will also be shown.

The calculated cohesive energies relative to that of diamond, and bond lengths in various polytypes of carbon, ranging from the dimer molecule to fcc structure, are presented in Fig. 1, in comparison with experimental data (for dimer, graphite and diamond) [17–19] or first-principles calculations (for simple cubic, bcc and fcc) [20]. The results from the Tersoff potential [1] are also compared. It is seen that the variations in energy and bond length with varying coordination number are equally well described by the present MEAM and the Tersoff potential. The relative cohesive energy difference from diamond, and lattice parameters, a and c, of graphite are reported to be about −0.02 eV/atom [17], and 2.46–2.47 Å and 6.71–6.93 Å [19], respectively. It should be mentioned here that the present potential gives many slightly different graphite structures with similar values of the cohesive energy and lattice parameters. The graphitic structures observed using the present potential are rhombohedral graphite and simple graphite as well as the ordinary hexagonal graphite. The calculated relative cohesive energy difference from diamond and the lattice parameters, a and c, of the rhombohedral graphite, simple graphite and the hexagonal graphite are listed in Table 2. Even for the hexagonal graphite, slightly different structures could be obtained, depending on the initial structure of the energy minimization. Furthermore, a converged value of cohesive energy could not be obtained for each structure. This made it difficult to calculate elastic constants (C_{11}, C_{33} etc.) using the atomistic approach. The same convergence problem also occurred for the rhombohedral graphite. On the other hand, well-defined atomic structures and converged energy values were obtained for the simple graphite structure. Therefore, in the present study, all calculations of elastic, defect and surface properties of graphite were performed on the basis of the simple graphite structure. Even though simple graphite is not a real graphitic structure, it is believed that the computation error arising from this choice would be small because the interlayer interaction

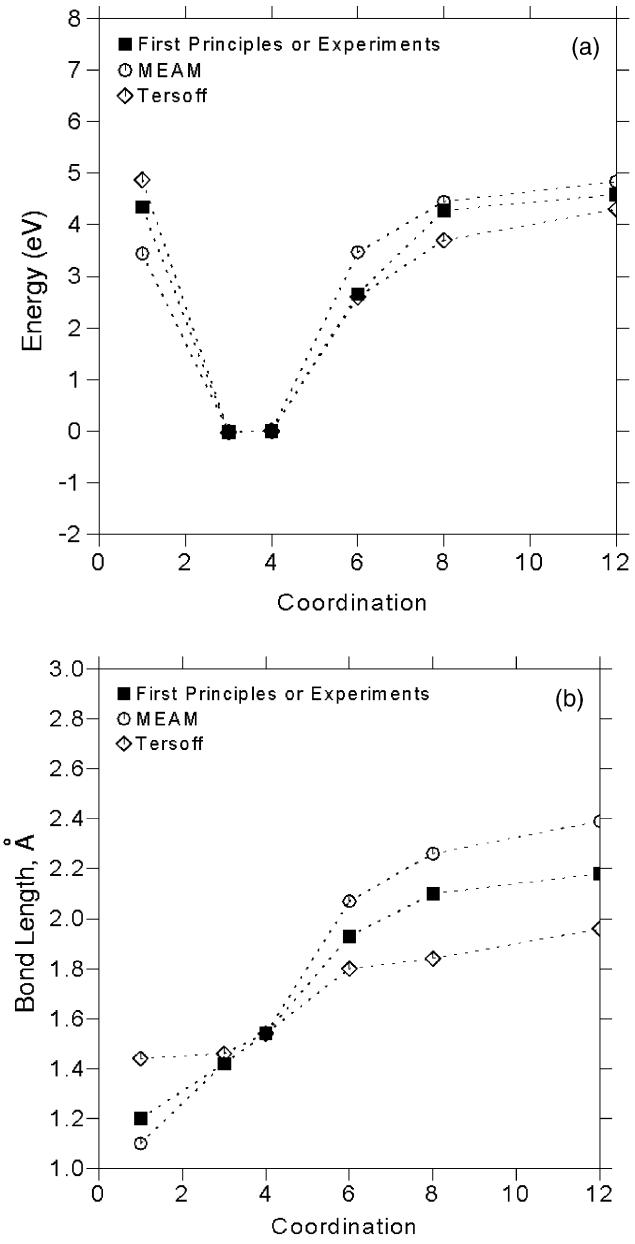

Fig. 1. Comparisons between the present calculation and experimental data or first-principles calculation for (a) cohesive energies relative to that of diamond and (b) bond lengths in various polytypes of carbon, ranging from the dimer molecule to fcc structure, versus atomic coordination number. The experimental data for cohesive energies for dimer, graphite and diamond are from Ref. [17], while those for the bond length of dimer, and graphite and diamond are from Refs. [18] and [19], respectively. The data for hypothetical structures of carbon (sc, bcc, fcc) are from first-principles calculations [20]. The results from the Tersoff potential [1] are also compared.

in graphite is small (<1%) compared to the in-plane interaction.

Table 3 shows physical properties of diamond calculated using the present MEAM potential, in comparison with calculations using the Tersoff potential, and experiments or other higher level or empirical calculations. The elastic constants are well reproduced by both the present and the

Table 1
Parameters for the MEAM and Lennard-Jones potentials of carbon

E_c	r_e	B	A	$\beta^{(0)}$	$\beta^{(1)}$	$\beta^{(2)}$	$\beta^{(3)}$	$t^{(1)}$	$t^{(2)}$	$t^{(3)}$	C_{max}	C_{min}	d	ε	σ
7.37	1.54	4.446	1.18	4.25	2.80	2.00	5.00	3.20	1.44	−4.48	2.80	1.41	0.00	0.03	3.1

The units of the cohesive energy E_c, the equilibrium nearest-neighbor distance r_e and the bulk modulus B are eV, Å and 10^{12} dyn/cm^2, respectively. The units of ε and σ are eV and Å, respectively.

Table 2
The relative cohesive energy difference from diamond and the lattice parameters, a and c, of rhombohedral graphite, simple graphite and hexagonal graphite, calculated using the present MEAM + L-J potential, in comparison with experimental data on the ordinary hexagonal graphite

	Rhombohedral graphite	Simple graphite	Hexagonal graphite	Exp.
$\Delta E_{gra/dia}$	−0.01	+0.01	−0.003	−0.02[a]
Lattice parameter, a	2.45	2.45	2.45	2.46–2.47[b]
Lattice parameter, c	6.63	6.95	6.66	6.71–6.93[b]

[a] Ref. [17].
[b] Ref. [19].

Tersoff potential, while the vacancy formation energies are lower compared to a first-principles calculation [23]. The split vacancy formation energy corresponds to the diffusion energy barrier based on a vacancy mechanism. According to the present potential, the tetrahedral and hexagonal self-interstitial atoms were unstable and transformed to (110) and (100) dumbbells, respectively, during energy minimization. For unrelaxed and relaxed surface energy and amount of relaxation of the surface layers, the present calculation shows a similar trend to the Tersoff potential. The agreements with first-principles calculations [24,25] and with another empirical calculation [26] are also good, except that the (111) surface energy from the higher level calculation [25] is much larger than those from all other empirical calculations. The distance between atoms in the relaxed (100) surface layer and the first subsurface layer was 1.45 Å, and the bond length of the dimer on the (2 × 1) reconstructed (100) surface was 1.48 Å. The corresponding values according to a first-principles calculation [24] are 1.47 and 1.37 Å, respectively.

The calculated thermal expansion coefficient and specific heat are around 8×10^{-6}/K and 25.5 J/mol K, respectively, with small temperature dependencies in the range of 300–1200 K. The corresponding experimental data [27] show larger temperature dependencies and smaller values than the present calculations in a similar temperature range. It should be noted here that the Debye temperature of elements is defined as the temperature above which the phonon mode can be regarded to be not quantized. Above the Debye temperature the phonon mode of materials can be described using the classical Boltzmann statistics. However, below the Debye temperature the phonon mode cannot be described correctly using the Boltzmann statistics, and should be described using other statistics (Bose–Einstein). The molecular dynamics using empirical interatomic potentials is based on the Boltzmann statistics, and is adequate for description of atomic-scale material behavior at above the Debye temperature. The Debye temperature of many elements is below or close to room temperature. Therefore, the thermal properties can be described correctly using classical molecular dynamics around the room temperature. However, the Debye temperature of diamond is extraordinarily high (1890 K). The temperature range 300–1200 K is not the range where the phonon mode of diamond can be described correctly using the present molecular dynamics based on an empirical interatomic potential. This is thought to be the reason for the poor agreement between calculation and experimental data on the thermal expansion coefficient and specific heat of diamond in the given temperature range (300–1200 K). The thermal property values obtained in the present calculation are rather close to the expected values on extrapolating the experimental data [27] to the Debye temperature of diamond. One needs to consider this discrepancy when performing a simulation where thermal properties can have decisive effects on the simulation results.

The calculated physical properties of graphite are compared in Table 4 with experimental data and other calculations. It should be mentioned here again that these calculations were performed using the present MEAM + L-J potential and were based on a simple graphite structure not the ordinary hexagonal graphite structure, due to the already mentioned convergence problem. When considering this approximation, the calculated elastic constant values are thought to be reasonable with an exception, C_{12}. The calculated vacancy formation energy and migration energy are also in good agreement with the first-principles calculation [31]. According to the present potential, the in-plane interstitial atoms (in hexagonal sites) were not stable and transformed to interlayer interstitial atoms. The calculated formation energy of the interlayer interstitial, 4.9 eV, is comparable to the experimental value 7 eV [32].

Table 3
Physical properties of diamond calculated using the present MEAM, in comparison with experimental data or other calculations

	MEAM	Tersoff	Exp./calc.
C_{11}	10.79	10.9[a]	10.80[c]
C_{12}	1.27	1.2[a]	1.27[c]
C_{44}	6.23	6.4[a]	5.77[c]
E_v^{f}	3.35	4.3[a]	7.2[d]
E_v^{split}	7.23	9.7[a]	9.1[d]
$E_{\mathrm{I(T)}}^{\mathrm{f}}$	Unstable	19.6[a]	23.6[d]
$E_{\mathrm{I(H)}}^{\mathrm{f}}$	Unstable	20.9[a]	–
$E_{\mathrm{I(110)db}}^{\mathrm{f}}$	12.7	–	–
$E_{\mathrm{I(100)db}}^{\mathrm{f}}$	9.3	10.0[a]	16.7[d]
$E_{\mathrm{ideal}}^{(100)}$	8811	7565[b]	9850[e], 9250[g]
$E_{\mathrm{ideal}}^{(110)}$	5715	4949[b]	6540[g]
$E_{\mathrm{ideal}}^{(111)}$	4666	4040[b]	7960[f], 5340[g]
$E_{1\times1}^{(100)}$	7124	6639[b]	9190[e]
$E_{2\times1}^{(100)}$	5720		5370[e]
$E_{1\times1}^{(111)}$	2069	2772[b]	6270[f]
$\Delta d_{1-2}^{(100)}$	−17.9	−15.9[b]	
$\Delta d_{2-3}^{(100)}$	+9.5	+2.0[b]	
$\Delta d_{1-2}^{(111)}$	−52.5	−39.8[b]	−49[f]
$\Delta d_{2-3}^{(111)}$	+21.1	+4.3[b]	+9[f]
ε (300–1200 K)	8		1–6[h]
C_p (300–1200 K)	25.5		5–22[h]

Values listed are the elastic constants C_{11}, C_{12}, C_{44}(10^{12} dyne/cm^2), the relaxed monovacancy and split vacancy formation energies E_v^{f} and E_v^{split} (eV), the relaxed tetrahedral, hexagonal, (110) dumbbell and (100) dumbbell interstitial formation energies $E_{\mathrm{I(T)}}^{\mathrm{f}}$, $E_{\mathrm{I(H)}}^{\mathrm{f}}$, $E_{\mathrm{I(110)db}}^{\mathrm{f}}$, $E_{\mathrm{I(100)db}}^{\mathrm{f}}$, the ideal (unrelaxed) (100), (110) and (111) surface energies $E_{\mathrm{ideal}}^{(100)}$, $E_{\mathrm{ideal}}^{(110)}$ and $E_{\mathrm{ideal}}^{(111)}$ (erg/cm^2), the 1×1 relaxed, 2×1 reconstructed surface energies of the (100) surface $E_{1\times1}^{(100)}$, $E_{2\times1}^{(100)}$, the 1×1 relaxed surface energy of the (111) surface $E_{1\times1}^{(111)}$, the relaxation of atomic layers Δd (%), the thermal expansion coefficient ε (10^{-6}/K), and the specific heat C_p (J/mol K). All calculations were carried out using a radial cutoff distance, 4 Å.

[a] Empirical calculation, Ref. [1].
[b] As calculated in Ref. [21].
[c] Experiment, Ref. [22].
[d] First-principles calculation, Ref. [23].
[e] First-principles calculation, Ref. [24].
[f] First-principles calculation, Ref. [25].
[g] Empirical calculation, Ref. [26].
[h] Experiment, Ref. [27].

The calculated surface energy showed a large anisotropy, 84 erg/cm^2 for the (0001) plane and 4000–5000 erg/cm^2 for other surfaces perpendicular to the (0001) plane.

In order to test the applicability of the present potential to atomistic studies on carbon nanotubes and fullerenes, some properties of carbon nanotubes (CNTs) and C_{60} (relative stabilities of graphene, some CNTs and C_{60}, and the elastic modulus and vacancy formation energy of CNTs) were also calculated. The results are given in Table 5, in comparison with experiments or other calculations. Though many more comparisons would have to be made before a conclusion can be drawn, the present results are certainly promising.

Finally, the properties of amorphous carbon were also investigated as was done by Tersoff [1]. The amorphous

Table 4
Physical properties of graphite calculated using the present MEAM + L-J potential, in comparison with experimental data or other calculations

	MEAM + L-J	Tersoff	Exp./calc.
B_{iso}	2.38	–	2.86[b]
C_{11}	10.99	12.1[a]	10.60[c]
C_{12}	−0.45	−1.9[a]	1.80[c]
C_{33}	0.38	–	0.365[c]
C_{44}	0.0003	–	0.04[c]
C_{13}	0.0003	–	0.15[c], −0.12[d], −0.005[e]
E_v^{f}	6.2	7.1[a]	7.6[f]
E_v^{split}	9.5	10.8[a]	9.2[f]
$E_{\mathrm{InterLayer}}^{\mathrm{f}}$	4.9	–	7.0[g]
$E_{(0001)}$	84		

Values listed are the isotropic bulk modulus B_{iso}(10^{12} dyne/cm^2), the elastic constants C_{11}, C_{12}, C_{33}, C_{44}, C_{13} (10^{12} dyne/cm^2), the relaxed monovacancy and split vacancy formation energies E_v^{f} and E_v^{split} (eV), the interlayer interstitial formation energy $E_{\mathrm{InterLayer}}^{\mathrm{f}}$ (eV), and the (0001) surface energy $E_{(0001)}$(erg/cm^2). All calculations were carried out using a cutoff distance 2.75 Å for MEAM and 5.75 Å for L-J, and for the simple graphite structure.

[a] Empirical calculation, Ref. [1].
[b] From elastic constants, Ref. [28].
[c] Experiment, Ref. [28].
[d] First-principles calculation, Ref. [29].
[e] First-principles calculation, Ref. [30].
[f] First-principles calculation, Ref. [31].
[g] Experiment, Ref. [32].

Table 5
Physical properties of graphene, some carbon nanotubes and C_{60} using the present MEAM + L-J potential, in comparison with experimental data or other calculations

	MEAM(+L-J)	Exp./calc.
ΔE of graphene	0.037	0.02[a], 0.045[b]
ΔE of (10,10) CNT	0.05	0.086[a], 0.10[b]
ΔE of (17,0) CNT	0.05	0.088[a], 0.10[b]
ΔE of C_{60} buckyball	0.59	0.46[a], 0.47[b]
Young's modulus of (10,10) CNT	10.4	10.02[c]
Vacancy formation energy in (8,0) CNT	5.71	5.59[d]

Values listed are the formation energy relative to diamond (eV), Young's modulus (10^{12} dyne/cm^2) and the vacancy formation energy (eV). All calculations were carried out using a cutoff distance, 2.75 Å for MEAM and 5.75 Å for L-J, but exactly the same results are obtained using only the MEAM potential.

[a] Graphite force field, Ref. [33].
[b] Reactive force field, Ref. [34].
[c] Average of eight experiments ranging from 3.2 to 14.7, Ref. [35].
[d] First-principles calculation, Ref. [36].

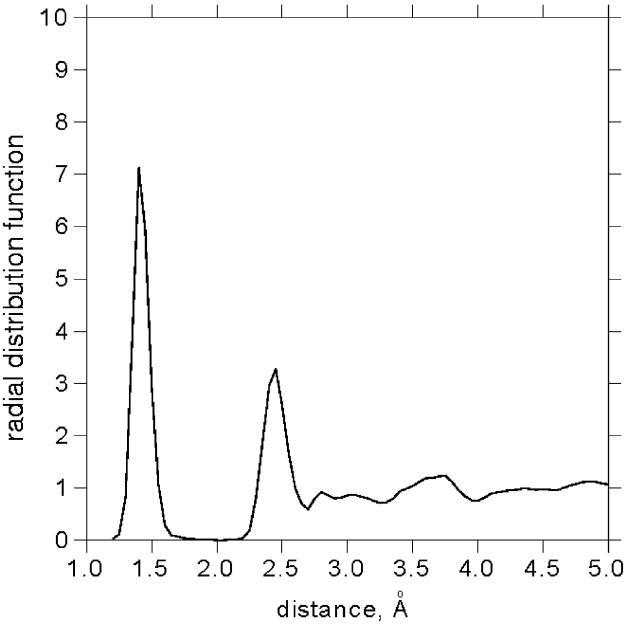

Fig. 2. Calculated radial distribution function of amorphous carbon obtained by rapidly cooling compressed liquid from 4800 to 300 K at a cooling rate of 8×10^{13} K/s, under zero-external-pressure conditions allowing relaxation.

carbon was prepared by rapidly cooling (2–8 $\times$ 10^{13} K/s) compressed liquid from 4800 to 300 K under a zero-external-pressure conditions allowing relaxation. It is known that a wide range of amorphous carbon (from graphitic to diamondlike) can be generated experimentally and also by simulation [37]. Available experimental information on graphitic amorphous carbon shows that the density is 0.4–0.6 of the diamond density and 1–10% of atoms are fourfold coordinated [38]. Radial distribution functions have also been derived experimentally [39,40]. According to the present simulation, the average energy per atom of the amorphous carbon was higher than that of diamond by about 0.43 eV. A small percentage of atoms were fourfold coordinated and slightly more than that were twofold coordinated, yielding an average coordination of 2.96. The corresponding value according to other empirical or higher level atomistic simulations ranges from 2.93 to 3.33 [1,37,41–43]. The average density of the amorphous carbon was calculated to be 0.58 of the diamond density. The average nearest-neighbor distance was very close to that of graphite (1.42 Å), and the peak in the bond angle distribution was located between 118° and 119° which is slightly lower than for graphite (120°). The calculated radial distribution function shown in Fig. 2 is in good agreement with experimental data [39] in the locations, heights and widths of the first and second peaks. As the cooling rate decreased the resultant atomic structure became closer to that of graphite in energy, average coordination, radial distribution and bond angle distribution.

It has been shown that the present MEAM interatomic potential for carbon can reproduce various physical properties of diamond and structural properties of various polytypes of carbon in good agreement with experiments or high level calculations. When combined with the Lennard-Jones potential, it can also reproduce the physical properties of graphite reasonably well. In general, it may be said that the reliability of the present MEAM potential is as good as that of the Tersoff potential for carbon [1]. A big difference between the present potential and the Tersoff potential is that the present potential can be easily combined with other MEAM potentials for metallic elements to describe various metal–carbon systems. The present authors already confirmed that the present potential can be successfully applied to the Fe–C and Ti–C systems [15], being combined with a separately developed MEAM potential for Fe [9] and Ti [44].

4. Conclusion

An MEAM interatomic potential for carbon that describes the structural properties of various polytypes of carbon, and elastic, defect and surface properties of diamond as satisfactorily as the well-known Tersoff potential has been developed. Combined with the Lennard-Jones potential, it can also reproduce physical properties of graphite, carbon nanotubes and fullerenes reasonably well. Because the potential formalism is the same as other already developed MEAM potentials for bcc, fcc and hcp elements, it can be easily extended to describe various metal–carbon binary systems.

Acknowledgements

The valuable discussions with Dr. Hanchul Kim and Dr. In-Ho Lee at KRISS, and Dr. Sang Soo Han at KAIST during the preparation of the present manuscript are greatly appreciated. This work was financially supported by the Ministry of Science and Technology of Korea through the National R&D Project for Nano Science and Technology (Grant No. M1-0213-04-0002).

Appendix

The formalism of the (2NN) MEAM for pure elements will now be briefly presented. It has been shown in Eq. (1) that the energy in the MEAM is composed of two terms, the embedding function term and the pair interaction term.

The embedding function is given the following form [10]:

$$F(\overline{\rho}) = AE_{\mathrm{c}}\frac{\overline{\rho}}{\overline{\rho}^{o}}\ln\frac{\overline{\rho}}{\overline{\rho}^{o}} \tag{A.1}$$

where A is an adjustable parameter, E_{c} is the cohesive energy and $\overline{\rho}^{o}$ is the background electron density for a reference structure. The reference structure is a structure where individual atoms are on the exact lattice points. Normally, the equilibrium structure is taken as the reference

structure for elements. The background electron density $\overline{\rho}_i$ is composed of the spherically symmetric partial electron density, $\rho_i^{(0)}$, and angular contributions, $\rho_i^{(1)}$, $\rho_i^{(2)}$, $\rho_i^{(3)}$. Each partial electron density term has the following form [10,45]:

$$(\rho_i^{(0)})^2 = \left[\sum_{j\neq i} S_{ij}\rho_j^{a(0)}(R_{ij})\right]^2 \tag{A.2a}$$

$$(\rho_i^{(1)})^2 = \sum_{\alpha}\left[\sum_{j\neq i}\frac{R_{ij}^{\alpha}}{R_{ij}} S_{ij}\rho_j^{a(1)}(R_{ij})\right]^2 \tag{A.2b}$$

$$(\rho_i^{(2)})^2 = \sum_{\alpha,\beta}\left[\sum_{j\neq i}\frac{R_{ij}^{\alpha}R_{ij}^{\beta}}{R_{ij}^2} S_{ij}\rho_j^{a(2)}(R_{ij})\right]^2 - \frac{1}{3}\left[\sum_{j\neq i} S_{ij}\rho_j^{a(2)}(R_{ij})\right]^2 \tag{A.2c}$$

$$(\rho_i^{(3)})^2 = \sum_{\alpha,\beta,\gamma}\left[\sum_{j\neq i}\frac{R_{ij}^{\alpha}R_{ij}^{\beta}R_{ij}^{\gamma}}{R_{ij}^3} S_{ij}\rho_j^{a(3)}(R_{ij})\right]^2 - \frac{3}{5}\sum_{\alpha}\left[\sum_{j\neq i}\frac{R_{ij}^{\alpha}}{R_{ij}} S_{ij}\rho_j^{a(3)}(R_{ij})\right]^2. \tag{A.2d}$$

Here, $\rho_j^{a(h)}$ represent atomic electron densities from j atom at a distance R_{ij} from site i. R_{ij}^{α} is the α component of the distance vector between atoms j and i ($\alpha = x, y, z$). The expression for $(\rho_i^{(3)})^2$ (Eq. (A.2d)) is that recently modified in order to make the partial electron densities orthogonal [45]. The way of combining the partial electron densities to give the total background electron density is not unique, and several expressions have been proposed [14]. Among them, the following form that can be widely used without numerical error is taken in the present work:

$$\overline{\rho}_i = \rho_i^{(0)} G(\Gamma) \tag{A.3}$$

where

$$G(\Gamma) = \frac{2}{1+\mathrm{e}^{-\Gamma}} \tag{A.4}$$

and

$$\Gamma = \sum_{h=1}^{3} t_i^{(h)}\left[\frac{\rho_i^{(h)}}{\rho_i^{(0)}}\right]^2 \tag{A.5}$$

and $t_i^{(h)}$ are adjustable parameters. The atomic electron density is given as

$$\rho_j^{a(h)}(R) = \rho_0 \mathrm{e}^{-\beta^{(h)}(R/r_\mathrm{e}-1)} \tag{A.6}$$

where ρ_0 is a scaling factor, $\beta^{(h)}$ are adjustable parameters and r_e is the nearest-neighbor distance in the equilibrium reference structure. The scaling factor does not have any effect on calculations for elements, but can have an effect on calculations for alloy systems.

In the MEAM no specific functional expression is given directly to $\phi(R)$. Instead, the atomic energy (total energy per atom) is evaluated by some means as a function of the nearest-neighbor distance. Then, the value of $\phi(R)$ is computed from known values of the total energy and the embedding energy, as a function of the nearest-neighbor distance.

Let us consider a reference structure once again. Here, every atom has the same environment and the same energy. If up to second-nearest-neighbor interactions are considered as is done in the second-nearest-neighbor MEAM [8,9], the total energy per atom in a reference structure can be written as follows:

$$E^a(R) = F(\overline{\rho}^o(R)) + \frac{Z_1}{2}\phi(R) + \frac{Z_2 S}{2}\phi(aR) \tag{A.7}$$

where Z_1 and Z_2 are the number of first- and second-nearest-neighbor atoms, respectively. S is the screening factor for second-nearest-neighbor interactions (the screening factor for first-nearest-neighbor interactions is 1), and a is the ratio between the second- and first-nearest-neighbor distances. It should be noted that for a given reference structure S and a are constants, and the total energy and the embedding energy become functions of only the nearest-neighbor distance R. On the other hand, the energy per atom for a reference structure can be obtained from the zero-temperature universal equation of state given by Rose et al. [13] as a function of nearest-neighbor distance R:

$$E^u(R) = -E_\mathrm{c}(1 + a^* + da^{*3})\mathrm{e}^{-a*} \tag{A.8}$$

where d is an adjustable parameter, and

$$a^* = \alpha(R/r_\mathrm{e} - 1) \tag{A.9}$$

and

$$\alpha = \left(\frac{9B\Omega}{E_\mathrm{c}}\right)^{1/2}. \tag{A.10}$$

$E^u(R)$ is the universal function for a uniform expansion or contraction in the reference structure, B is the bulk modulus and Ω is the equilibrium atomic volume.

Basically, the pair potential between two atoms separated by a distance R, $\phi(R)$, can be obtained by equating Eqs. (A.7) and (A.8). However, it is not trivial because Eq. (A.7) contains two pair potential terms. In order to derive an expression for the pair interaction, $\phi(R)$, another pair potential, $\psi(R)$, is introduced:

$$E^u(R) = F(\overline{\rho}^o(R)) + \frac{Z_1}{2}\psi(R) \tag{A.11}$$

where

$$\psi(R) = \phi(R) + \frac{Z_2 S}{Z_1}\phi(aR). \tag{A.12}$$

$\psi(R)$ can be computed from Eq. (A.11) as a function of R, as follows:

$$\psi(R) = \frac{2}{Z_1}[E^u(R) - F(\overline{\rho}^o(R))], \tag{A.13}$$

and the expression for the pair potential $\phi(R)$ is obtained from Eq. (A.12) as follows:

$$\phi(R) = \psi(R) + \sum_{n=1}(-1)^n \left(\frac{Z_2 S}{Z_1}\right)^n \psi(a^n R). \tag{A.14}$$

Here, the summation is performed until a correct value of the atomic energy is obtained for the equilibrium reference structure.

It should be noted here that the original first-nearest-neighbor MEAM is a special case ($S = 0$) of the present 2NN MEAM. In the original MEAM, the neglect of the second-nearest-neighbor interactions is effected by the use of a strong many-body screening function [14]. In the same way, the consideration of the second-nearest-neighbor interactions in the modified formalism is effected by adjusting the many-body screening function so that it becomes less severe. In the MEAM, the many-body screening function between atoms i and j, S_{ij}, is defined as the product of the screening factors, S_{ikj}, due to all other neighbor atoms k:

$$S_{ij} = \prod_{k \neq i,j} S_{ikj}. \tag{A.15}$$

The screening factor S_{ikj} is computed using a simple geometric construction. Imagine an ellipse on an x, y plane, passing through atoms, i, k and j with the x-axis of the ellipse determined by atoms i and j. The equation of the ellipse is given by

$$x^2 + \frac{1}{C}y^2 = \left(\frac{1}{2}R_{ij}\right)^2. \tag{A.16}$$

For each k atom, the value of parameter C can be computed from relative distances among the three atoms, i, j and k, as follows:

$$C = \frac{2(X_{ik} + X_{kj}) - (X_{ik} - X_{kj})^2 - 1}{1 - (X_{ik} - X_{kj})^2} \tag{A.17}$$

where $X_{ik} = (R_{ik}/R_{ij})^2$ and $X_{kj} = (R_{kj}/R_{ij})^2$. The screening factor, S_{ikj}, is defined as a function of C as follows:

$$S_{ikj} = f_c\left[\frac{C - C_{\min}}{C_{\max} - C_{\min}}\right] \tag{A.18}$$

where $C_{\min}$ and $C_{\max}$ are the limiting values of C determining the extent of screening and the smooth cutoff function is

$$f_c(x) = \begin{cases} 1 & x \geq 1 \\ \left[1 - (1-x)^4\right]^2 & 0 < x < 1 \\ 0 & x \leq 0. \end{cases} \tag{A.19}$$

The basic idea for the screening is as follows. First define two limiting values, $C_{\max}$ and $C_{\min}$ ($C_{\max} > C_{\min}$). Then, if the atom k is outside of the ellipse defined by $C_{\max}$, it is thought that the atom k does not have any effect on the interaction between atoms i and j. If the atom k is inside of the ellipse defined by $C_{\min}$ it is thought that the atom k completely screens the i–j interaction, and between $C_{\max}$ and $C_{\min}$ the screening changes gradually. In the numerical procedure of simulation the electron density and pair potential are multiplied by the screening function S_{ij}, as in done in Eqs. (1) and (A.2a)–(A.2d). Therefore, $S_{ij} = 1$ and $S_{ij} = 0$ mean that the interaction between atoms i and j is unscreened and completely screened, respectively. In addition to the many-body screening function, a radial cutoff function which is given by $f_c[(r_c - r)/\Delta r]$ where r_c is the cutoff distance and Δr (0.1 Å) is the cutoff region, is also applied to the atomic electron density and pair potential [14]. The radial cutoff distance is chosen so that it does not have any effect on the calculation results due to the many-body screening. This is only for computational convenience, that is, to save computation time.

References

[1] J. Tersoff, Phys. Rev. Lett. 61 (1988) 2879.
[2] D.W. Brenner, Phys. Rev. B 42 (1990) 9458.
[3] M.I. Heggie, J. Phys.: Condens. Matter 3 (1991) 3065.
[4] E.P. Andribet, J. Domínguez-Vázquez, A. Mari Carmen Pérez-Martín, E.V. Alonso, J.J. Jiménez-Rodríquez, Nucl. Instrum. Methods Phys. Res. B 115 (1996) 501.
[5] J. Tersoff, Phys. Rev. Lett. 56 (1986) 632; Phys. Rev. B 37 (1988) 6991; Phys. Rev. B 38 (1988) 9902.
[6] J. Tersoff, Phys. Rev. B 39 (1989) 5566.
[7] D.W. Brenner, O.A. Shenderova, J.A. Harrison, S.J. Stuart, B. Ni, S.B. Sinnott, J. Phys.: Condens. Matter 14 (2002) 783.
[8] B.-J. Lee, M.I. Baskes, Phys. Rev. B 62 (2000) 8564.
[9] B.-J. Lee, M.I. Baskes, H. Kim, Y.K. Cho, Phys. Rev. B 64 (2001) 184102.
[10] M.I. Baskes, Phys. Rev. B 46 (1992) 2727.
[11] M.S. Daw, M.I. Baskes, Phys. Rev. Lett. 50 (1983) 1285; Phys. Rev. B 29 (1984) 6443.
[12] S.M. Foiles, M.I. Baskes, M.S. Daw, Phys. Rev. B. 33 (1986) 7983.
[13] J.H. Rose, J.R. Smith, F. Guinea, J. Ferrante, Phys. Rev. B 29 (1984) 2963.
[14] M.I. Baskes, Mater. Chem. Phys. 50 (1997) 152.
[15] B.-J. Lee, Pohang University of Science and Technology, Korea, Unpublished work, 2004.
[16] B.-J. Lee, J.-H. Shim, M.I. Baskes, Phys. Rev. B 68 (2003) 144112.
[17] L.B. Pankratz, Thermodynamic properties of elements and oxides, US Bureau of Mines, Bulletin 672, 1982.
[18] W.A. Harrison, Phys. Rev. B 27 (1983) 3592.
[19] P. Villars, L.D. Calvert, Pearson's Handbook of Crystallographic Data for Intermetallic Phases, ASM International, Materials Park, OH, 1991.
[20] M.T. Yin, M.L. Cohen, Phys. Rev. Lett. 50 (1983) 2006; Phys. Rev. B 29 (1984) 6996.
[21] T. Halicioglu, Surf. Sci. Lett. 259 (1991) L714.
[22] R. Vogelgesang, A.K. Ramdas, S. Rodriguez, M. Grimsditch, T.R. Anthony, Phys. Rev. B 54 (1996) 3989.
[23] J. Bernholc, A. Antonelli, T.M. Del Sole, Y. Bar-Yam, S.T. Pantelides, Phys. Rev. Lett. 61 (1988) 2689.
[24] J. Furthmüller, J. Hafner, G. Kresse, Phys. Rev. B 53 (1996) 7334.
[25] G. Kern, J. Hafner, G. Kresse, Surf. Sci. 366 (1996) 445.
[26] S. Terentiev, Diam. Relat. Mater. 8 (1999) 1444.
[27] C. Moelle, S. Klose, F. Szücs, H.J. Fecht, C. Johnston, P.R. Chalker, M. Werner, Diam. Relat. Mater. 6 (1997) 839.
[28] O.L. Blakslee, D.G. Proctor, E.J. Seldin, G.B. Spence, T. Weng, J. Appl. Phys. 41 (1970) 3373.
[29] H.J.F. Jansen, A.J. Freeman, Phys. Rev. B 35 (1987) 8207.
[30] J.C. Boettger, Phys. Rev. B 55 (1997) 11202.

[31] E. Kaxiras, K.C. Pandey, Phys. Rev. Lett. 61 (1988) 2693.
[32] P.A. Thrower, R.M. Mayer, Phys. Status Solidi a 47 (1978) 11.
[33] Y. Guo, N. Karasawa, W.A. Goddard III, Nature 351 (1991) 464.
[34] K.D. Nielson, A.C.T. van Duin, J. Oxgaard, W.-Q. Deng, W.A. Goddard III, J. Phys. Chem. A 109 (2005) 493.
[35] M.-F. Yu, B.S. Files, S. Arepalli, R.S. Ruoff, Phys. Rev. Lett. 84 (2000) 5552.
[36] S.B. Fagan, L.B. da Silva, R. Mota, Nano Lett. 3 (2003) 289.
[37] P.C. Kelires, Phys. Rev. B 47 (1993) 1829.
[38] J. Robertson, Adv. Phys. 35 (1986) 317.
[39] F. Li, J.S. Lannin, Phys. Rev. Lett. 65 (1990) 1905.
[40] S. Kugler, K. Shimakawa, T. Watanabe, K. Hayashi, I. László, R. Bellissent, J. Non-Cryst. Solids 164–166 (1993) 1143.
[41] C.Z. Wang, K.M. Ho, C.T. Chan, Phys. Rev. Lett. 70 (1993) 611.
[42] U. Stephan, M. Haase, J. Phys. Condens. Matter 5 (1993) 9157.
[43] G. Galli, R. Martin, R. Car, M. Parinello, Phys. Rev. Lett. 62 (1989) 555.
[44] Y.M. Kim, B.-J. Lee, Pohang University of Science and Technology, Korea, Unpublished work, 2004.
[45] M.I. Baskes, Mater. Sci. Eng. A 261 (1999) 165.